

Frequency Augmented Clock Synchronization for Space-based interferometry

Abel, Felix ; Sundaramoorthy, Prem; Rajan, R.T.

Publication date

2022

Document Version

Accepted author manuscript

Citation (APA)

Abel, F., Sundaramoorthy, P., & Rajan, R. T. (2022). *Frequency Augmented Clock Synchronization for Space-based interferometry*. Paper presented at 4S Symposium 2022, Vilamoura, Portugal.

Important note

To cite this publication, please use the final published version (if applicable).
Please check the document version above.

Copyright

Other than for strictly personal use, it is not permitted to download, forward or distribute the text or part of it, without the consent of the author(s) and/or copyright holder(s), unless the work is under an open content license such as Creative Commons.

Takedown policy

Please contact us and provide details if you believe this document breaches copyrights.
We will remove access to the work immediately and investigate your claim.

FREQUENCY AUGMENTED CLOCK SYNCHRONIZATION FOR SPACE-BASED INTERFEROMETRY

Felix Abel, Prem Sundaramoorthy, Raj Thilak Rajan*

Faculty of EEMCS, Delft University of Technology (TUD), Delft, The Netherlands

Abstract

Recently, an increase in distributed space systems and a rise in number of nodes in such systems is observed in numerous space applications, for example space-based interferometry. Such applications pose stringent demands on time synchronization which can be challenging to achieve for satellite networks that lack an absolute time reference source, as would be the case with networks beyond Earth orbit. In this paper, we propose a new class of frequency-based and multi-domain time synchronization and ranging algorithms applicable to anchorless mobile networks of asynchronous nodes. First, the Frequency-based Pairwise Least Squares (FPLS) that estimates clock skew and relative velocity under constant pairwise velocity assumption. Second, the Combined Pairwise Least Squares (CPLS) — a two step approach where first, skew and velocity are estimated using FPLS and then its results are fed into a reformulated time domain method to estimate offset and range. The proposed methods are applied to a case study to OLFAR — a spaceborne large aperture radio interferometric array platform for observing the cosmos in the frequency range from 0.3 MHz to 30 MHz to be stationed in the Lunar orbit. The results show that the proposed methods decrease communication and computation needs and can improve the clock synchronization performance for space-based interferometry.

1 INTRODUCTION

Asynchronous networks are characterized by the lack of an absolute time reference, and mobile networks are furthermore challenging due to the relative motion between the nodes. In such a network, the distances and hence message propagation delays change within the period required to synchronize the nodes. Establishing time synchronization among the nodes, however, is crucial in enabling applications such as interferometry or localization. Such networks commonly have limited available energy resources. It is thus desirable to decrease communication and processing needed to achieve synchronization among nodes using pairwise synchronization algorithms. By improving and augmenting prevalent algorithms [1, 2], this paper aims to contribute to make future space arrays, and sensor networks at large, more energy efficient and more widely applicable.

Among network time synchronization methods one can distinguish between pairwise methods and global methods. Pairwise methods synchronize a network by synchronizing pairs of nodes with one another whereas global methods compute a solution for the whole network in a centralized algorithm [3, ch. 4]. This work will limit its scope to pairwise methods because of their linear complexity with number of nodes in the network, their lower computational requirements, and their inherently distributed nature.

*Dr.ir. Prem Sundaramoorthy and Dr. R.T.Rajan are partially funded partially by the Dutch-PIPP (Partnerships for Space Instruments Applications Preparatory Programme), funded by NWO (Netherlands Organisation for Scientific Research) and NSO (Netherlands Space Office)

Current algorithms for time synchronization in anchorless networks of mobile asynchronous nodes rely solely on measuring time stamps of exchanged messages. The main contribution this paper aims to make in the field of time synchronization algorithms is the use of frequency domain methods to augment existing time domain methods.

In this paper, we propose a class of frequency-based and multi-domain time synchronization and ranging algorithms applicable to an anchorless mobile network of asynchronous nodes and demonstrate their applicability for space-based interferometry. To harness the full potential of frequency domain synchronization and ranging, we further propose the Combined Pairwise Least Squares (CPLS) — a two stepped approach where first, skew and velocity are estimated using Frequency Pairwise Least Squares (FPLS) and then, second, its results are fed into a reformulated time domain method to estimate offset and range. Finally, the proposed methods are applied to a case study of OLFAR. We show through simulations, that the proposed method can significantly improve the clock synchronization performance for space-based interferometers.

Notation: Upper-case variables (A) and lower-case variables (a) denote scalars, bold lower-case (\mathbf{a}) denote vectors, bold upper-case (\mathbf{A}) denote matrices and $(\mathbf{1}_N)$ is a column vector of ones of size $N \times 1$. The \odot operator denotes the Hadamard or element-wise matrix product, $(\cdot)^{\odot N}$ element-wise exponential, $(\cdot)^\dagger$ the Moore-Penrose pseudo inverse and $\langle \cdot \rangle$ the expected value of a random variable.

2 RELATED WORK

Time synchronization of inherently asynchronous nodes is a key challenge in wireless sensor networks. Where available, external time references such as a Global Navigation Satellite System (GNSS) can be used to achieve time synchronization, however, there are applications with limited or no access to an absolute time and position reference, e.g. in space beyond Earth orbit, dense urban environments, underwater or indoor applications. In such anchorless networks, where the lack of an external reference prevents absolute synchronization, relative synchronization among the nodes can be achieved.

2.1 Two Way Ranging

The affine clock model and the concept of two way ranging (TWR) using time measurements are the underlying concept used in prevalent time domain methods [1, 2, 3, 4, 5]. The affine clock model represents the local time at node i

$$t_i = \omega_i t + \phi_i \quad \Leftrightarrow \quad \mathcal{C}_i(t_i) \triangleq t = \alpha_i t_i + \beta_i \quad (1)$$

where the clock parameters are uniquely related to the clock parameters as $[\alpha_i, \beta_i] \triangleq [\omega_i^{-1}, -\phi_i \omega_i^{-1}]$ and $\mathcal{C}_i(t_i)$ expresses true time as a function of local time [3, ch. 4]. For the scope of this paper, clock parameters are assumed to be constant over the maximum coherence time $\tau_{c,max}$ and the synchronization period $t_r \ll \tau_{c,max}$ that the network takes to estimate clock parameters to be small compared to the maximum coherence time [6].

To synchronize their clocks, let two nodes i and j exchange time-stamped messages. As transmission is not instantaneous, there is a delay between a message being time-stamped by the transmitter i and the receiver j . This delay commonly consists of deterministic and stochastic terms and modeling them correctly is critical for good performance of the time synchronization algorithm. Following the notation of [3, ch. 4] and expressing the delay in terms of local times measured during message exchange we get for the k -th transmission,

$$E_{ij,k} \tau_k = \mathcal{C}_j(T_{ji,k}) - \mathcal{C}_i(T_{ij,k}) \quad \text{for } i \leftrightarrow j \quad (2)$$

where $E_{ji,k}$ indicates the direction of transmission as

$$E_{ij,k} = \begin{cases} +1 & i \rightarrow j \\ -1 & i \leftarrow j \end{cases} \quad (3)$$

and $T_{ij,k}$ and $T_{ji,k}$ are the timestamps collected at node i and j respectively and τ_k is the delay at the k -th transmission. Expressing equation (3) in terms of calibration parameters,

$$E_{ij,k}\tau_k = \alpha_j T_{ji,k} + \beta_j - \alpha_i T_{ij,k} - \beta_i, \quad (4)$$

where $E_{ij,k}$, $T_{ij,k}$ and $T_{ji,k}$ are known and the clock parameters α and β are to be estimated.

2.2 Mobile Pairwise Least Squares

The optimal joint estimation of clock offset and skew under known delays τ_k for a fixed immobile network of nodes was demonstrated by Noh et al. in [4], where the delays τ_k were assumed to be composed of a known delay component τ (constant over the synchronization period) and a stochastic component η_k . Wu et al. considered a scenario with constant but unknown propagation delay between the nodes for the duration of all K communications [1, 5]. As the unknown delay is required for clock parameter estimation, it is inevitable to estimate the propagation delay. Hence, this algorithm is not merely a time synchronization method but rather a joint synchronization and ranging method.

In an effort to improve synchronization and ranging performance for networks of mobile nodes, Rajan and van der Veen presented a class of more advanced synchronization techniques by extending the stationary Low Complexity Least Squares (LCLS) to a motion model that assumes constant velocity [7] or even constant acceleration [8]. A universal formulation employing an L -th order motion model was presented by the same authors in [3, ch. 4], [2], namely Mobile Pairwise Least Squares (MPLS) and Mobile Global Least Squares (MGLS). Higher-order motion models significantly improved the estimation performance for mobile anchorless networks and are applicable even for non-linear pairwise motion. For this class of algorithms, the varying delay is modeled as

$$\tau_k = \gamma_{ij}^{(0)} + \gamma_{ij}^{(1)}T_{ij,k} + \gamma_{ij}^{(2)}T_{ij,k}^2 + \dots + \gamma_{ij}^{(L-1)}T_{ij,k}^{L-1} + \eta_{ij,k} \quad (5)$$

where L is the order of the algorithm and $\gamma_{ij}^{(\cdot)}$ are the translated range parameters of the Taylor series expansion. The translated range parameters $\gamma_{ij}^{(\cdot)}$ are uniquely related to the range parameters (distance, velocity, acceleration, ...). $\eta_{ij,k}$ is an i.i.d. zero mean Gaussian random variable representing the stochastic delay component. As shown in [3], (4) can then be extended to

$$\begin{bmatrix} \mathbf{t}_{ij} & -\mathbf{t}_{ji} & \mathbf{1}_K & -\mathbf{1}_K & \text{diag}(\mathbf{e}_{ij}) \mathbf{V}_{ij} \\ \gamma_{ij}^{(0)} \\ \vdots \\ \gamma_{ij}^{(L-1)} \end{bmatrix} = \boldsymbol{\eta}_{ij}, \quad (6)$$

where $\mathbf{t}_{ij} = [T_{ij,1}, T_{ij,2}, \dots, T_{ij,K}]^T$, $\mathbf{e}_{ij} = [E_{ij,1}, E_{ij,2}, \dots, E_{ij,K}]^T$, $\boldsymbol{\tau}_{ij} = [\tau_{ij,1}, \tau_{ij,2}, \dots, \tau_{ij,K}]^T$ and $\mathbf{V}_{ij} = \begin{bmatrix} \mathbf{t}_{ij}^{\odot 0} & \mathbf{t}_{ij}^{\odot 1} & \mathbf{t}_{ij}^{\odot 2} & \dots & \mathbf{t}_{ij}^{\odot L-1} \end{bmatrix}$ is the Vandermonde matrix. Choosing either one of the two nodes as

as a reference node e.g., node i , one can then solve in a least squares sense for the remaining $L + 2$ unknowns. For the problem to be solvable, $K \geq 2 + L$ must hold for the number of communications and communication must be bi-directional, e.g. at least one message in each direction [3, p. 74].

2.3 On global and pairwise methods

Besides the pairwise method, Rajan and van der Veen proposed global methods for time synchronization. More specifically, a stationary global method was presented in [9] and a mobile global formulation in [2],[3, ch. 4]. Global formulations like the MGLS algorithm solve the time synchronization and ranging problem for the whole network of nodes rather than in a pairwise manner. This formulation lead to a block-incidence-matrix-like structure in a system of equations that is initially under-determined for lack of a clock reference. In [3, ch. 4], several equality constrained least squares formulations have been proposed to solve this optimization problem. The possibility of choosing a virtual average clock as reference via the constraints (sum constraint, see [3, p. 85]) rather than a reference node as in pairwise methods can lead to improvements in clock parameter estimation. Furthermore, global methods can exploit information gathered on all $0.5N(N - 1)$ pairwise links which further contributes to the superior performance of global algorithms in fully connected networks. In contrast, existing pairwise methods are by design only able to make use of $N - 1$ links. Nonetheless, pairwise methods are computationally less demanding as they scale linearly with network size requiring $N - 1$ pairwise synchronizations where each pairwise operation is evidently independent of network size. The computational complexity of global methods for large networks is given as $\mathcal{O}(KN^2L^2)$ [3, p. 81]. Global algorithms are centralized, meaning they lend themselves well to Master/Slave configurations where a centralized node collects all data, computes the result to then distribute it to the nodes. MGLS is distributable [3, p. 81], however the distributed version will require additional communication between nodes and further increase implementation complexity. Given the disadvantages of global methods regarding failure tolerance, implementation complexity and energy requirements, this work will exclusively focus on pairwise synchronization methods.

2.4 Other related work

Note, that besides the prevalent methods specifically for anchorless mobile networks, a plethora of time synchronization algorithms exist for wireless sensor networks (WSNs) in general as synchronization and ranging is a field of active research. For example in [10], Kazaz et al. use phase difference of arrival (PDoA) measurements of narrowband signals for synchronization in stationary IoT networks incorporating offset and skew effects. Wang et al. propose a clock skew estimator based on passive listening in [11]. In [12], Zhu et al. propose an innovative synchronization method based on reaching distributed consensus between the nodes of the network. However, none of these three methods operate on mobile networks. For mobile networks, recent advances have been made by Gu et al. who built on top of the MGLS algorithm from [2], and proposed a synchronous two-way ranging based on pseudo range measurements thereby reducing computational complexity [13].

3 FREQUENCY DOMAIN SYNCHRONIZATION

The concept of augmenting time domain information with frequency domain information is frequently used in wireless sensing applications, for example in Doppler radars [14] or Doppler tracking of spacecraft by ground stations [15, 16]. In addition, timing and ranging applications also exploit frequency information e.g., in frequency difference of arrival (FDOA) ranging applications [17]. Another example is [18], where frequency information is used in the context of clock synchronization of stationary wireless

sensor networks, however, frequency information is used in here as a binary indicator for the synchronization status of the clocks in the network rather than for clock parameter estimation. Among the prior work in this area, [19] comes closest to the application of interest in this paper. In their work, Roehr et al. exploit frequency domain information for clock synchronization in a pairwise scenario. However, their approach is limited to stationary nodes and requires a coarse pre-synchronization of node clocks. In this paper, we exploit the fact that the Doppler shift on the communication between the nodes in a mobile network is due to both the relative motion and their respective clock skews ω_i , are these parameters are directly related to the frequencies transmitted and received by the nodes.

3.1 Frequency domain two way ranging

In this subsection, a framework for frequency domain two-way ranging is proposed by relating the transmitted and received frequencies between two nodes exchanging messages, to their clock parameters and relative motion. Let an electromagnetic wave be sent from transmitter to a receiver that is moving w.r.t the transmitter. The Doppler frequency — the frequency shift due to relative motion — can be expressed as $f_d = f_r - f_t$ where f_t and f_r are the transmitted frequency and received frequency respectively. For small Doppler velocities $|v_d| \ll c$, the Doppler velocity — for the scope of this work typically $0 < |v_d| < 10^3 \frac{\text{m}}{\text{s}}$ in magnitude — can be expressed as $v_d = \frac{f_d}{f} c$ where c is the propagation speed of the wave — for the scope of this work speed of light — and f is the frequency of the wave without Doppler shift. For an application like OLFAR, a possible frequency f could be S-band at 3GHz which would lead to Doppler frequencies of $0 < |f_d| < 10\text{kHz}$. A relation between the clock parameters of an arbitrary node i and the frequency f_i it generates is established. First, the frequency of an electromagnetic wave is related to its period, Δt_i , as

$$f = \frac{1}{\Delta t}, \quad f_i = \frac{1}{\Delta t_i}. \quad (7)$$

Furthermore, let us express this time delay as a function of the local time delay using equation (1) for the affine clock model:

$$\Delta t = \mathcal{C}_i(t_i + \Delta t_i) - \mathcal{C}_i(t_i) = \alpha_i(t_i + \Delta t_i) + \beta_i - \alpha_i t_i - \beta_i = \alpha_i \Delta t_i \quad (8)$$

As expected, when trying to generate the wave with period Δt_i , the true period will be Δt dependent on the clock skew, not the offset. Thirdly, we can express this relation in terms of frequencies and clock skew ω_i as

$$f = \omega_i f_i. \quad (9)$$

Equation (9) shows that when node i set to generate the frequency f_i , the clock skew ω_i at the node affects the true frequency f generated. Now, let a message be sent from node i to j . The transmission frequency $F_{ij,k}$ is selected at the transmitting node i when transmitting to node j , where subscript k indicates the index of the message. It is then affected by the clock skew ω_i as described in (9). Due to the relative motion of the nodes, the transmission is subject to Doppler shift $f_{d,k}$ which can be expressed as a the difference between true received frequency and true transmitted frequency as

$$f_{d,k} = \omega_j F_{ji,k} - \omega_i F_{ij,k} \quad \text{for } i \rightarrow j, \quad (10)$$

where $F_{ji,k}$ in this case is the received frequency measured at node j . More generally, we can write for bi-directional communication with added Gaussian noise

$$E_{ij,k} f_{d,k} + \omega_i F_{ij,k} - \omega_j F_{ji,k} = \eta_k \quad \text{for } i \leftrightarrow j, \quad (11)$$

where $\eta_k \sim \mathcal{N}(0, \sigma^2)$ and $E_{ij,k} = +1$ for transmission from i to j and $E_{ij,k} = -1$ for transmission from j to i . The noise is assumed to be zero mean Gaussian.

3.2 Frequency-based Pairwise Least Squares

Assuming a constant Doppler velocity v_d for all k one can express (11) in terms of velocity rather than Doppler frequency as

$$\begin{aligned} & \frac{v_d}{c} (G_{ij,k} \omega_i F_{ij,k} - G_{ji,k} \omega_j F_{ji,k}) + \\ & \omega_i F_{ij,k} - \omega_j F_{ji,k} = \eta_k \quad \text{for } i \leftrightarrow j, \end{aligned} \quad (12)$$

where the first term expresses the Doppler frequency. The binary variable

$$G_{ij,k} = \begin{cases} 1 & i \rightarrow j \\ 0 & i \leftarrow j \end{cases}, \quad G_{ji,k} = \begin{cases} 0 & i \rightarrow j \\ 1 & i \leftarrow j \end{cases}, \quad (13a)$$

$$\mathbf{g}_{ij} = [G_{ij,1}, G_{ij,2}, \dots, G_{ij,K}]^T \in \mathbb{Z}_2^{K \times 1} \quad (13b)$$

denotes an indicator. The scalar frequency measurements of K transmissions can be stacked into a measurement vector as $\mathbf{f}_{ij} = [F_{ij,1}, F_{ij,2}, \dots, F_{ij,K}]^T \in \mathbb{R}^{K \times 1}$. Rewriting (12) for K communications and assuming node i as clock reference i.e., $\omega_i^{-1} \triangleq 1$, the equation simplifies to

$$\begin{bmatrix} -\mathbf{f}_{ji} & c^{-1} \mathbf{g}_{ij} \odot \mathbf{f}_{ij} & -c^{-1} \mathbf{g}_{ji} \odot \mathbf{f}_{ji} \end{bmatrix} \begin{bmatrix} \omega_j \\ v_d \\ v_d \omega_j \end{bmatrix} + \mathbf{f}_{ij} = \boldsymbol{\eta}_{ij}. \quad (14)$$

Assuming the noise vector $\boldsymbol{\eta}_{ij}$ to be i.i.d. zero mean Gaussian, equation (14) can be solved in a least squares sense for the clock skew $\hat{\omega}_j$ of node j , the relative velocity \hat{v}_d and their product, leading to the Frequency Pairwise Least Squares (FPLS) algorithms. For this solution to hold the following requirements must be met:

1. There must be bi-directional communication between the nodes.
2. The number of messages fulfills $K \geq 3$.
3. Requirements 1 and 2 imply that at least one node must transmit at least two messages to the other. The transmit frequencies of these two messages have to be different from one another.

The synchronization algorithms based on frequency-domain measurements differ from the time-domain methods in several ways. The clock offset cannot be estimated using Frequency Pairwise Least Squares (FPLS), but the clock skew can be estimated without concern for the offset. Similarly, it allows a direct estimation of the relative velocity, while being unable to obtain the propagation delay. For some applications where offset and delay/distance are not of interest, using the frequency domain method can be beneficial over using time domain methods. However, the attribute of frequency domain methods to only operate on skew and velocities are a limitation with respect to the application of anchorless networks of mobile asynchronous nodes where it is required to estimate both clock skew and offset. Thus, the proposed FPLS cannot fully replace those algorithms based on time measurements. Instead, we propose the Combined Pairwise Least Squares (CPLS) in the next section employing FPLS to augment and improve the performance of time domain algorithms.

4 MULTI-DOMAIN SYNCHRONIZATION

To overcome the limitation of Frequency Pairwise Least Squares (FPLS), we propose a two-stepped approach, wherein FPLS is used to estimate clock skew and relative velocity, and then use a modified MPLS of order L to estimate distance and skew. From (6), the equation for the Mobile Pairwise Least Squares with $L = 2$ is

$$\begin{bmatrix} \mathbf{t}_{ij} & -\mathbf{t}_{ji} & \mathbf{1}_K & -\mathbf{1}_K & \mathbf{e}_{ij} & \mathbf{e}_{ij} \odot \mathbf{t}_{ij} \end{bmatrix} \begin{bmatrix} \alpha_i \\ \alpha_j \\ \beta_i \\ \beta_j \\ \gamma_{ij}^{(0)} \\ \gamma_{ij}^{(1)} \end{bmatrix} = \boldsymbol{\eta}_{ij}. \quad (15)$$

Similar to all pairwise methods, the calibration parameters of the reference node is assigned $\alpha_i = 1, \beta_i = 0$. Next, the algorithm is modified to include prior results from frequency domain. Let $\alpha_j \triangleq \hat{\omega}_j^{-1}$ and $\gamma_{ij}^{(1)} \triangleq \hat{\gamma}_{ij}^{(1)} = c^{-1}\alpha_i\hat{v}_d$. Then, the known and unknown quantities in equation (15) can be separated as

$$\begin{bmatrix} -\mathbf{1}_K & \mathbf{e}_{ij} \end{bmatrix} \begin{bmatrix} \beta_j \\ \gamma_{ij}^{(0)} \end{bmatrix} = \begin{bmatrix} -\mathbf{t}_{ij} & \mathbf{t}_{ji} & -\mathbf{e}_{ij} \odot \mathbf{t}_{ij} \end{bmatrix} \begin{bmatrix} 1 \\ \hat{\omega}_j^{-1} \\ \hat{\gamma}_{ij}^{(1)} \end{bmatrix} \quad (16)$$

which can be solved for $K \geq 2$ bi-directional communications. In conclusion, in a combined time-frequency methods using equations (14) and (16), both clock parameters and dynamic parameters of up to velocity order can be estimated requiring only three messages between the nodes. For this method to work, the requirements for FPLS given in the respective subsection must be fulfilled.

5 CLOCK SYNCHRONIZATION IN SPACE-BASED INTERFEROMETRY

We now look at an application of clock synchronization for space-based interferometry, and in particular OLFAR, which stands for Orbiting Low Frequency Array for Radio astronomy [20]. Its concept has been developed in the last decade by a group of universities and research institutions in the Netherlands, which aims to augment the capabilities of the ground-based Low-Frequency Array (LOFAR) operated by the Netherlands Institute for Radio astronomy (ASTRON) [21]. The use case for OLFAR is to provide a space-borne large aperture radio interferometric array platform in a frequency range from 0.3 MHz to 30 MHz [22, 23]. By stationing OLFAR in space far away from Earth, in Lunar orbit or Earth-Moon L2, interference from Earth can be mitigated [23]. OLFAR is proposed to consist of a swarm of ≥ 10 satellites [22], but the exact number of elements varies across the different publications. The performance of OLFAR as distributed radio telescope is strongly dependent on achieving time synchronization among its nodes. If a chosen clock for the OLFAR project fulfils the Allan deviation requirement i.e. remaining stable during the integration time [3, ch. 3], then we can safely assume that during the coherence period τ_c , the residual synchronization errors will be dominant over higher order clock effects [6]. For OLFAR, the requirement was set forth that during a snapshot integration time, baseline distance should not change by more than 0.1λ (observed wavelength) [24] which for $\lambda = 10\text{m}$ leads to a maximum total clock error of $\delta t_i = 3.33\text{ns}$. As this is the requirement for the snapshot integration time of 1s, achieving it for the whole synchronization period of $> 1\text{s}$ will satisfy the clock accuracy requirement. The re-synchronization threshold is chosen such that when the total clock error of the nodes in the network exceeds δt_i , a re-synchronization has to be performed.

Several different deployment locations for OLFAR are discussed in [25]. Among the more recent publications on OLFAR, Lunar orbit has emerged as a preferred deployment location [26], largely thanks to its proximity to Earth which will minimize communication requirements for the downlink. Besides, among the possible deployment locations, the highest orbital velocities and the highest relative velocities between the nodes are expected. This means, if a satisfactory clock synchronization performance can be achieved for this scenario, it shows the feasibility also for other less demanding deployment locations.

5.1 Relative Orbital motion in Lunar orbit

Various works have been carried out on OLFAR orbit design, most notably by Dekens et al. in 2013 [24], van t’Hoff [27] and Mok et al. in 2020 [28]. Neither of those works propose an orbit design in Lunar orbit that satisfies all requirements of the OLFAR mission. Dekens et al. propose orbits that fail to meet the baseline rate requirement of OLFAR. Mok et al. address this issue, proposing a new set of algebraic constraints under which the original requirements are met, but they do not propose specific orbit parameters to fulfil these. Thus, this work will follow [24] and use their approach to OLFAR orbit design. Despite its violation of some of the OLFAR mission requirements it is sufficient for the purpose of validating time synchronization techniques.

The requirements for orbit design follow from the general mission requirements and science objectives as the imaging performance is tightly linked to the relative orbital motion. OLFAR requires an angular resolution θ of 1 arcminute, following $\theta = \frac{\lambda}{B}$ where B is the largest baseline distance and λ the observed wavelength [29]. It was found by [24] that a relative orbital design where all satellites drift freely within a sphere of 100km without active orbit determinations is sufficient for achieving the baseline requirement of the mission. Furthermore, during the snapshot integration time (time over which one measurement is taken), the baseline distance should not change by more than 0.1λ (observed wavelength) which for $\lambda = 30\text{m}$ leads to a resultant maximum relative velocity (baseline rate) of $3\frac{\text{m}}{\text{s}}$. This potentially conflicts with the coverage requirement stating that a high variation in spacial configuration over the mission duration is beneficial for imaging quality and thus desirable [24]. For a swarm in Lunar orbit with the aforementioned baseline and baseline rate requirements, these two are fundamentally incompatible as shown by [24], thus a relaxation of one of the requirements might be necessary for OLFAR.

Nevertheless, Dekens et al. proposed two orbits for OLFAR where baseline rates of $116\frac{\text{m}}{\text{s}}$ and $30\frac{\text{m}}{\text{s}}$ are achieved for orbit heights of 200km and 3000km respectively. The orbit radius is composed of the radius of Moon r_M and the orbit height h_O as $a = r_M + h_O$. While these orbits violate the baseline rate requirement, the increased pairwise velocity makes the time synchronization effort more difficult. The potential options to meet OLFAR mission requirements include relaxing the snapshot integration time and thus the baseline rate requirement, decreasing coverage requirements, introducing active orbit control or choosing a different staging location. All of these options would if at all lead to a decrease in pairwise velocities compared to the two orbits proposed in [24] and therefore relax the requirements for time synchronization. Hence, if the performance of time synchronization algorithms can be demonstrated for these two orbital scenarios it can be concluded that the time synchronization techniques will meet OLFAR requirements.

Dekens et al. use the HCW equations in a de-rotated Hill frame, called sky frame. Compared to the Hill frame that is oriented relative to the reference orbit, the sky frame is oriented relative to the fixed stars. In [24], this representation is used to gauge the imaging performance of OLFAR. The positions in

Table 1: Boundaries on relative orbital parameters taken from [24] with baseline $B = 100km$ and orbit radius a

Parameter	Minimum	Maximum
α	0	0
β	$-\frac{B}{2a}$	$\frac{B}{2a}$
γ	0	0
δ	0	$\frac{B}{2a}$
ξ	0	2π
ψ	0	2π

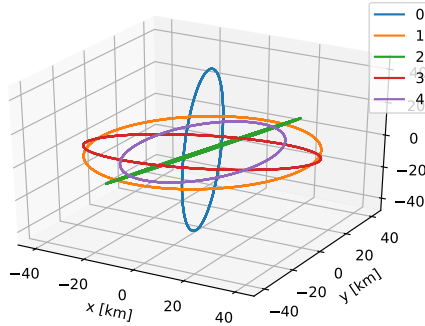


Figure 1: Sky frame HCW 3D track for 200km orbit height for $N = 5$ nodes for 1 orbital period

a Cartesian coordinate systems as a function of time are given as described in equations (17).

$$x(t) = -a\beta \sin(tn) \quad (17a)$$

$$y(t) = a\beta \cos(tn) \quad (17b)$$

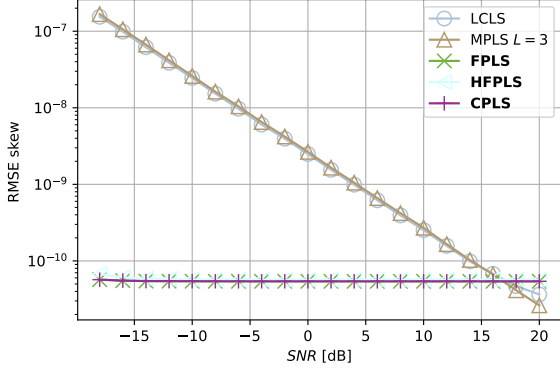
$$z(t) = a\delta \sin(tn - \psi) \quad (17c)$$

Parameters α , β , γ , δ , ξ and ψ are the relative semi-major axis, relative anomaly, relative eccentricity, relative inclination, relative periapsis and relative ascending node respectively [30, 24] and a is the radius of the circular reference orbit.

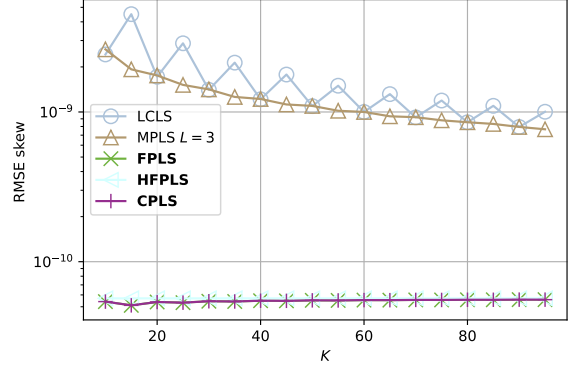
For OLFAR to meet its baseline requirements, Dekens et al. chose these parameters as shown in table 1, and initialized the parameters of N satellites as uniform random distributed over the allowed interval. Figure 1 shows the results of a realization of (17) with parameters from table 1 in a 3D view. As expected, the equations lead to orbital planes of varying orientations, semi-major and semi-minor axes.

6 SIMULATION RESULTS

This section validates the proposed clock synchronization methods based on frequency measurements, and, furthermore to compare their performance to existing time-domain algorithms. The estimation performance for time and frequency of departure and arrival depends on receiver architecture, clock hardware, ADC hardware, the estimator as well frequency, bandwidth, signal duration, noise on the wireless channel and waveform of the signal used for transmission. Thus, the accuracy of time and frequency measurements is highly dependant on the respective communication system. Note, that time and



(a) Clock skew ω estimation error for $K = 10$



(b) clock skew ω estimation error for SNR = 0dB

Figure 2: Clock skew estimation for varying number of measurements K and for varying SNR

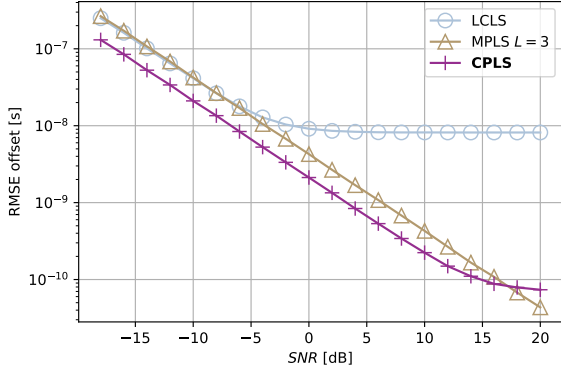
frequency measurement accuracy might be affected differently by some system parameters, e.g. high bandwidth caters to higher TOA measurement accuracy while being less important for frequency measurements. Without loss of generality, we assume the noise on the time and frequency markers to be i.i.d. zero mean Gaussian. We define the standard deviation of the time domain noise as $\sigma_t = c^{-1}10^{\frac{-\text{SNR}}{10}}$, where SNR is the SNR in dbMeter. The frequency domain noise standard deviation is defined as $\sigma_f = \frac{(f_{min}+f_{max})\bar{v}}{2\bar{d}c}10^{\frac{-\text{SNR}}{10}}$, where \bar{d} and \bar{v} are the mean relative distance and velocity between then nodes respectively.

6.1 Choice of parameters

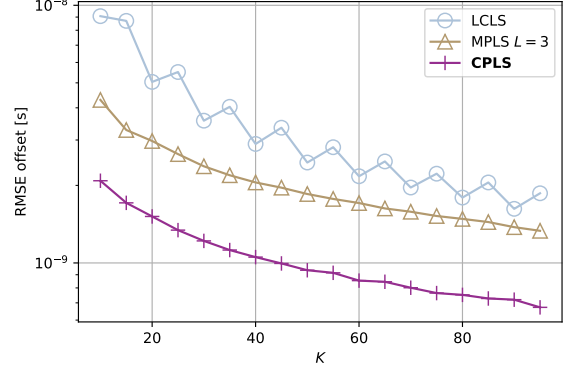
In this simulation, $N = 5$ nodes are simulated. For the simulation of the orbital motion of the OLFAR nodes, the Sky-HCW-model is used. Out of the two orbital designs presented by Dekens et al. the one with the lower orbital height of 200km is selected, as the lower orbit leads to higher relative velocities between the nodes compared to the a higher orbit. The clock errors are uniformly distributed with parameters $|\phi| \leq 5\text{s}$ on the clock offset and $|\omega| \leq 10^{-5}$ on the skew. The message exchange takes place between $t_{min} = 0\text{s}$ and $t_{max} = 3\text{s}$. The target transmission frequencies will be varied from $f_{min} = 0.9 \times 3 \times 10^9\text{Hz}$ to $f_{max} = 1.1 \times 3 \times 10^9\text{Hz}$ corresponding to S-band. The default SNR is set to 0dB and the number of pairwise communications is set to $K = 10$ as default.

6.2 Results and Analysis

We conduct simulations for varying SNR and number of communications K to illustrate the effect of both parameters on the root mean square error (RMSE) on the various algorithms. The algorithms proposed in this work are highlighted with **bold font** in the legend. In Figure 2a, it can be observed that the skew estimation of time domain methods improves with higher SNR while the frequency domain methods attain a low error also for low SNR. For significantly high SNR, the time domain methods improve even beyond the frequency domain methods. For varying K in Figure 2b, it can be seen that time domain methods benefit from increased K . However, for larger K , the improvement that additional number of communications can deliver decreases. The observation that at SNR = 0dB frequency domain methods are superior to mobile time domain methods which in turn are superior over the stationary LCLS in terms of offset estimation can be confirmed for the whole K range depicted.



(a) clock offset ϕ estimation error for $K = 10$



(b) clock offset ϕ estimation error for SNR = 0dB

Figure 3: Clock offset estimation for varying number of measurements K and for varying SNR

As frequency domain methods are by nature unable to estimate offset, existing time domain algorithms are represented alongside the proposed Combined Pairwise Least Squares (CPLS). The results for existing time domain methods are in line with prior results by [3, ch. 4]. In 3a, it can be observed that for low and medium SNR the combined method achieves superior performance over time domain methods. As the offset and distance estimations of CPLS are based on frequency domain skew and velocity measurements, where the frequency domain methods achieve superior performance, it is plausible that these superior estimates plugged into CPLS are the cause for its superiority in offset estimation. Furthermore, the SNR from where MPLS with $L = 3$ achieves better offset estimation (17dB) coincides with that SNR where it starts to outperform FPLS/CPLS in skew estimation. Looking at the 0dB SNR cut for varying K in Figure 3b, it can be seen that all methods benefit from increased K , however, for larger K , the improvement that additional number of communications can deliver decreases. The observation that at SNR = 0dB CPLS is superior to mobile time domain methods which in turn are superior over LCLS in terms of offset estimation can be confirmed for the whole K range depicted.

We now aim to determine the re-synchronization period for the OLFAR mission. Following equation (1), let the total clock error of the i -th node be defined as

$$\begin{aligned}\delta t_i(t) &= t - t_i \\ \delta t_i(t) &= t - (1 + \delta\omega_i)t + \delta\phi_i \\ \delta t_i(t) &= \delta\omega_i t + \delta\phi_i,\end{aligned}\tag{18}$$

where t is the true time elapsed since the beginning of the last synchronization and $\delta\omega_i$ and $\delta\phi_i$ are the clock skew and clock offset estimation errors respectively. As previously discussed, for OLFAR, the maximum acceptable local clock error is $|\delta t_i(t)| = 3.33\text{ns}$. Now, re-synchronization period t_r can be found by solving the previous equation for the true time t .

$$t_r = \frac{\delta t_i - \langle |\delta\phi_i| \rangle}{\langle |\delta\omega_i| \rangle},\tag{19}$$

where, the maximum acceptable local clock error is specified and the expected absolute values for the clock errors are known from simulations. We simulate a scenario with $K = 10$ messages. The required re-synchronization period can then be shown as a function of the SNR. The results are shown in Figure 4. Consider a SNR of 10dB. Using CPLS a re-synchronization period of 180s could be achieved, whereas the prevalent method MPLS with $L = 3$ only allows for a 40s re-synchronization period. Moreover, the

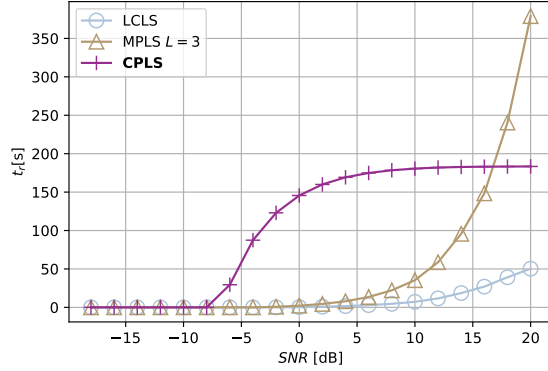


Figure 4: Re-synchronization period t_r for the OLFAR mission with $K = 10$, and varying SNR at $\delta t_i(t) = 10\text{ns}$ for the satellite array at orbit height of 200km.

figure shows that the novel CPLS outperforms prevalent methods particularly in low to medium SNR conditions, whereas in higher SNR conditions MPLS with $L = 3$ can outperform CPLS. The fact that CPLS is going into saturation can be attributed to the residual bias in the skew estimate.

It is anticipated, that one complete synchronization cycle will take in the order of few seconds depending on the synchronization path planning method chosen and the required processing and guard times between messages. At a re-synchronization period of 180s with CPLS, only a small fraction of the mission time will be required for synchronization purposes, and the OLFAR system will be available for scientific work during most of the mission time. It was furthermore important to show that the re-synchronization period is much larger than the snapshot integration time of 1s, which was herewith achieved. Besides, in section 2 it was determined that the coherence time of the clock hardware must be larger than the synchronization period. In [3, ch. 3], suitable clock hardware exceeding 1000s coherence time for OLFAR requirements was presented. Thus, the re-synchronization periods of 180 seconds are well in line with available clock hardware.

7 CONCLUSIONS

In this paper, we presented a class of novel frequency and multi domain algorithms for pairwise timing and ranging was proposed and tested through simulation. The proposed methods decrease communication cost, computational effort and can improve estimation performance over prevalent time domain algorithms. They are widely applicable to stationary and mobile wireless sensor network (WSN)s in various network configurations. The decrease in communication and computational requirements and increase in estimation performance can lower cost, mass and energy consumption for WSNs and potentially enable new applications with demanding requirements on clock parameter estimation. Furthermore, we simulated our proposed algorithms for the use case of the OLFAR mission. It was found that the proposed CPLS and prevalent MPLS can achieve satisfactory synchronization performance in the most challenging dynamic conditions possible for the OLFAR mission. A design space for number of nodes and their associated time to synchronize has been derived. The work can serve as a basis for system level trade-offs between number of nodes, synchronization time, node capability and re-synchronization frequency in the context of the OLFAR mission and other satellite constellations.

References

- [1] M. Leng and Y. Wu, “On clock synchronization algorithms for wireless sensor networks under unknown delay,” *IEEE Transactions on Vehicular Technology*, vol. 59, no. 1, pp. 182–190, 2010.
- [2] R. T. Rajan and A.-J. van der Veen, “Joint ranging and synchronization for an anchorless network of mobile nodes,” *IEEE Transactions on Signal Processing*, vol. 63, no. 8, pp. 1925–1940, 2015.
- [3] R. T. Rajan, *Relative Space-Time Kinematics of an Anchorless Network*, 3rd ed., 2016.
- [4] K. Noh, Q. M. Chaudhari, E. Serpedin, and B. W. Suter, “Novel clock phase offset and skew estimation using two-way timing message exchanges for wireless sensor networks,” *IEEE Transactions on Communications*, vol. 55, no. 4, pp. 766–777, 2007.
- [5] Y. Wu, Q. Chaudhari, and E. Serpedin, “Clock synchronization of wireless sensor networks,” *IEEE Signal Processing Magazine*, vol. 28, no. 1, pp. 124–138, 2011.
- [6] R. T. Rajan, M. Bentum, and A.-J. Boonstra, “Synchronization for space based ultra low frequency interferometry,” in *2013 IEEE Aerospace Conference*. IEEE, 2013, pp. 1–8.
- [7] R. T. Rajan and A.-J. van der Veen, “Joint motion estimation and clock synchronization for a wireless network of mobile nodes,” in *2012 IEEE International Conference on Acoustics, Speech and Signal Processing (ICASSP)*, 2012, pp. 2845–2848.
- [8] R. T. Rajan and A.-J. van der Veen, “Joint non-linear ranging and affine synchronization basis for a network of mobile nodes,” in *21st European Signal Processing Conference (EUSIPCO 2013)*, 2013, pp. 1–5.
- [9] —, “Joint ranging and clock synchronization for a wireless network,” in *2011 4th IEEE International Workshop on Computational Advances in Multi-Sensor Adaptive Processing (CAMSAP)*, 2011, pp. 297–300.
- [10] T. Kazaz, M. Coutino, G. J. M. Janssen, G. Leus, and A.-J. van der Veen, “Joint ranging and clock synchronization for dense heterogeneous iot networks,” in *2018 52nd Asilomar Conference on Signals, Systems, and Computers*, 2018, pp. 2169–2173.
- [11] H. Wang, H. Zeng, and P. Wang, “Linear estimation of clock frequency offset for time synchronization based on overhearing in wireless sensor networks,” *IEEE Communications Letters*, vol. 20, no. 2, pp. 288–291, 2016.
- [12] L. Zhu, S. Shi, and X. Gu, “A consensus-based distributed clock synchronization for wireless sensor network,” in *2018 14th International Wireless Communications Mobile Computing Conference (IWCMC)*, 2018, pp. 828–832.
- [13] X. Gu, G. Zhou, J. Li, and S. Xie, “Joint time synchronization and ranging for a mobile wireless network,” *IEEE Communications Letters*, vol. 24, no. 10, pp. 2363–2366, 2020.
- [14] M. A. Richards, J. A. Scheer, and W. A. Holm, *Principles of Modern Radar, Volume I - Basic Principles*. SciTech Publishing, 2010.
- [15] K. Cheung, D. Divsalar, and S. Bryant, “Two-way ranging and doppler for multiple orbiting spacecraft at mars,” in *2018 IEEE Aerospace Conference*, 2018, pp. 1–17.

- [16] J. R. Jensen and R. S. Bokulic, "Highly accurate, noncoherent technique for spacecraft doppler tracking," *IEEE Transactions on Aerospace and Electronic Systems*, vol. 35, no. 3, pp. 963–973, 1999.
- [17] K. Ho and Y. Chan, "Geolocation of a known altitude object from TDOA and FDOA measurements," *IEEE Transactions on Aerospace and Electronic Systems*, vol. 33, no. 3, pp. 770–783, 1997.
- [18] C. Bo, D. Enqing, L. Xiaoyang, Z. Dejing, and W. Jiaren, "A time synchronization algorithm based on bimodal clock frequency estimation," in *2012 18th Asia-Pacific Conference on Communications (APCC)*, 2012, pp. 75–78.
- [19] S. Roehr, P. Gulden, and M. Vossiek, "Method for high precision clock synchronization in wireless systems with application to radio navigation," in *2007 IEEE Radio and Wireless Symposium*, 2007, pp. 551–554.
- [20] R. T. Rajan, M. Bentum, and A. Boonstra, "Synchronization for space based ultra low frequency interferometry," in *2013 IEEE Aerospace Conference*, 2013, pp. 1–8.
- [21] M. Bentum, M. Verma, R. Rajan, A. Boonstra, C. Verhoeven, E. Gill, A. van der Veen, H. Falcke, M. K. Wolt, B. Monna, S. Engelen, J. Rotteveel, and L. Gurvits, "A roadmap towards a space-based radio telescope for ultra-low frequency radio astronomy," *Advances in Space Research*, vol. 65, no. 2, pp. 856–867, 2020, high-resolution space-borne radio astronomy.
- [22] R. T. Rajan, S. Engelen, M. Bentum, and C. Verhoeven, "Orbiting low frequency array for radio astronomy," in *2011 Aerospace Conference*, 2011, pp. 1–11.
- [23] S. Engelen, C. Verhoeven, and M. Bentum, "Olfar, a radio telescope based on nano satellites in moon orbit," in *24th Annual Conference on Small Satellites*. Utah State University, Aug. 2010, pp. 1–7.
- [24] E. Dekens, S. Engelen, and R. Noomen, "A satellite swarm for radio astronomy," *Acta Astronautica*, vol. 102, pp. 321–331, 2014.
- [25] R. Rajan, A. Boonstra, and M. e. a. Bentum, "Space-based aperture array for ultra-long wavelength radio astronomy," *Exp Astron*, vol. 41, p. 271–306, 2016.
- [26] V. Karunanithi, R. T. Rajan, P. Sundaramoorthy, M. Verma, C. Verhoeven, M. Bentum, and E. McCune, "High data-rate inter-satellite link (ISL) for space-based interferometry," in *70th International Astronautical Congress*, oct 2019.
- [27] J. A. van 't Hoff, *Numerical optimisation of constellation and orbit design for the OLFAR radio interferometry swarm in orbit of the Earth-Moon L4 point.*, 2020. [Online]. Available: <https://repository.tudelft.nl/islandora/object/uuid%3Ae1dd90a2-3130-49ba-aa13-0a436536e4dd>
- [28] S. H. Mok, J. Guo, E. Gill, and R. T. Rajan, "Lunar orbit design of a satellite swarm for radio astronomy," in *2020 IEEE Aerospace Conference*, 2020, pp. 1–9.
- [29] S. Jester and H. Falcke, "Science with a lunar low-frequency array: From the dark ages of the universe to nearby exoplanets," *New Astronomy Reviews*, vol. 53, no. 1, pp. 1–26, 2009.
- [30] S. D'Amico, "Autonomous formation flying in low earth orbit," Ph.D. dissertation, Delft University of Technology, 2010, nEO.